Potent mouse monoclonal antibodies that block SARS-CoV-2 infection

Received for publication, December 27, 2020, and in revised form, January 12, 2021 Published, Papers in Press, January 30, 2021,
https://doi.org/10.1016/j.jbc.2021.100346

Youjia Guo[1], Atsushi Kawaguchi[2,3,4], Masaru Takeshita[5], Takeshi Sekiya[2], Mikako Hirohama[2], Akio Yamashita[6], Haruhiko Siomi[1,*], and Kensaku Murano[1,*]

From the [1]Department of Molecular Biology, Keio University School of Medicine, Tokyo, Japan; [2]Department of Infection Biology, Faculty of Medicine, [3]Transborder Medical Research Center, and [4]Microbiology Research Center for Sustainability, University of Tsukuba, Tsukuba, Japan; [5]Division of Rheumatology, Department of Internal Medicine, Keio University School of Medicine, Tokyo, Japan; [6]Department of Molecular Biology, Yokohama City University School of Medicine, Yokohama, Japan

Edited by Karin Musier-Forsyth

Coronavirus disease 2019 (COVID-19), caused by severe acute respiratory syndrome coronavirus 2 (SARS-CoV-2), has developed into a global pandemic since its first outbreak in the winter of 2019. An extensive investigation of SARS-CoV-2 is critical for disease control. Various recombinant monoclonal antibodies of human origin that neutralize SARS-CoV-2 infection have been isolated from convalescent patients and will be applied as therapies and prophylaxis. However, the need for dedicated monoclonal antibodies suitable for molecular pathology research is not fully addressed. Here, we produced six mouse anti-SARS-CoV-2 spike monoclonal antibodies that not only exhibit robust performance in immunoassays including western blotting, ELISA, immunofluorescence, and immunoprecipitation, but also demonstrate neutralizing activity against SARS-CoV-2 infection to VeroE6/TMPRSS2 cells. Due to their mouse origin, our monoclonal antibodies are compatible with the experimental immunoassay setups commonly used in basic molecular biology research laboratories, providing a useful tool for future research. Furthermore, in the hope of applying the antibodies of clinical setting, we determined the variable regions of the antibodies and used them to produce recombinant human/mouse chimeric antibodies.

The outbreak of coronavirus disease 2019 (COVID-19) caused by severe acute respiratory syndrome coronavirus 2 (SARS-CoV-2) is a threat to global public health and economic development (1, 2). Vaccine and therapeutic discovery efforts are paramount to restrict the spread of the virus. Passive immunization could have a major effect on controlling the virus pandemic by providing immediate protection, complementing the development of prophylactic vaccines (3–5).

With the development of humanized mouse antibodies and subsequent generation of fully human antibodies by various techniques, monoclonal antibodies have become widely used in therapy and prophylaxis for cancer, autoimmune diseases, and viral pathogens (3). Indeed, a humanized mouse monoclonal antibody neutralizing respiratory syncytial virus (RSV), palivizumab, is widely used in clinical settings prophylactically to protect vulnerable infants (6). In recent years, highly specific and often broadly active neutralizing monoclonal antibodies have been developed against several viruses (3, 7–10). Passive immunization with a monoclonal antibody is currently under consideration as a treatment for COVID-19 caused by SARS-CoV-2 (4, 11–14).

Isolation of multiple human neutralizing monoclonal antibodies against SARS-CoV-2 has been reported (15–29). These antibodies can avoid the potential risks of human–anti-mouse antibody responses and other side effects (30). However, since they are recombinant human antibodies produced in HEK293 cell lines derived from human embryonic kidney, they have a disadvantage compared with conventional hybridoma-produced antibodies in terms of their lot-to-lot quality control and manufacturing costs (31). Instead, monoclonal antibodies produced by hybridomas are secreted into the culture supernatant, thus their production is straightforward and of low cost, and their quality is stable.

In addition to the impact of monoclonal antibodies on therapy and prophylaxis, they significantly impact the characterization of SARS-CoV-2. To overcome the long-term battle with the virus, we need a detailed understanding of the replication mechanisms underlying its life cycle, including viral entry, genome replication, budding from the cellular membrane, and interaction with host immune systems. These essential pieces of information are required for drug discovery, vaccine design, and therapy development. Despite the large number of neutralizing antibodies reported to inhibit infection, there is an overwhelming lack of data on a well-characterized antibody available for basic research techniques such as western blotting (WB), immunofluorescence, and immunoprecipitation to study the viral life cycle.

Here, we established six monoclonal antibodies against the spike glycoprotein of SARS-CoV-2. The trimeric spike glycoproteins of SARS-CoV-2 play a pivotal role in viral entry into human target cells through the same receptor, angiotensin-converting enzyme 2 (ACE2) as SARS-CoV-1 (32). We evaluated these antibodies for application in molecular pathology

* For correspondence: Haruhiko Siomi, awa403@keio.jp; Kensaku Murano, kmurano@keio.jp.

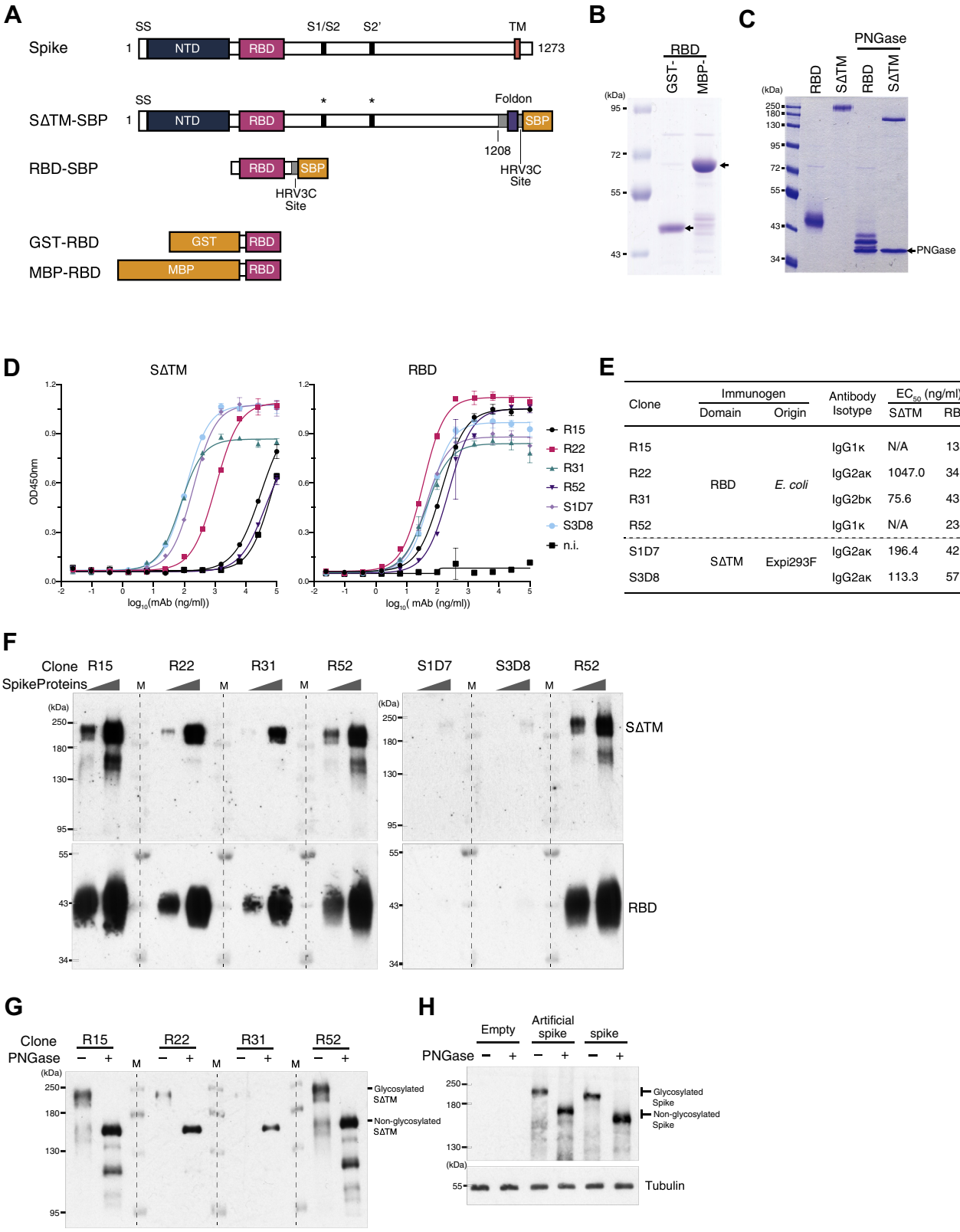

Clone	Immunogen		Antibody Isotype	EC_{50} (ng/ml)	
	Domain	Origin		SΔTM	RBD
R15	RBD	*E. coli*	IgG1κ	N/A	135.0
R22			IgG2aκ	1047.0	34.1
R31			IgG2bκ	75.6	43.0
R52			IgG1κ	N/A	234.6
S1D7	SΔTM	Expi293F	IgG2aκ	196.4	42.7
S3D8			IgG2aκ	113.3	57.7

Figure 1. Production of six monoclonal antibodies against spike protein. *A*, schematic of recombinant proteins used to establish anti-spike antibodies. For mammalian expression constructs (SΔTM-SBP and RBD-SBP), the HRV3C cleavage site was placed upstream of the SBP tag so that the SBP tag could be removed by HRV3C protease treatment after protein purification (Fig. S1*A*). *B*, Coomassie brilliant blue (CBB) staining of recombinant protein purified from *E. coli* expression system. GST-RBD and MBP-RBD appeared as bands of 46 kDa and 62 kDa, respectively. *C*, CBB staining of recombinant proteins purified from the mammalian expression system. The glycosylation of recombinant proteins caused smear bands and a lower migration rate of proteins on SDS-PAGE compared with proteins treated with PNGase. *D*, ELISA-binding affinity of purified monoclonal antibodies to trimeric SΔTM and RBD glycoproteins purified from the mammalian expression system. Error bars indicate standard deviation (n = 3). *E*, summary of isotype and EC_{50} of established monoclonal antibodies. *F*, Western blotting (WB) against SΔTM and RBD glycoproteins (10 or 50 ng per lane) using purified monoclonal antibodies (1 μg/ml in PBS-T).

research. Among them, two antibodies were shown to attenuate the interaction of spike proteins with ACE2 and neutralized infection of VeroE6/TMPRSS2 cells by SARS-CoV-2. Our antibodies will accelerate research on SARS-CoV-2 and lead to new therapies and prophylaxis.

Results

Production of six monoclonal antibodies against spike glycoprotein

The SARS-CoV-2 spike glycoprotein is a homotrimeric fusion protein composed of two subunits: S1 and S2. During infection, the receptor-binding domain (RBD) on S1 subunit binds to ACE2, resulting in destabilization of the spike protein's metastable conformation. Once destabilized, the spike protein is cleaved into the N-terminal S1 and C-terminal S2 subunits by host proteases such as TMPRSS2 and changes conformation irreversibly from the prefusion to the postfusion state (32–34), which triggers an infusion process mediated by the S2 region (35, 36). The instability needs to be addressed to obtain high-quality spike proteins for downstream applications. We adopted the design principle reported by Wrapp *et al.* (37), in which the SARS-CoV-2 spike protein was engineered to form a stable homotrimer that was resistant to proteolysis during protein preparation. In our practice, recombinant spike protein RBD and ectodomain were constructed. A T4 fabritin trimerization motif (foldon) was incorporated into the C terminal of the recombinant spike ectodomain to promote homotrimer formation (38) (Fig. 1*A*). Recombinant RBD proteins tagged with GST or MBP were produced using an *E. coli* expression system (Fig. 1*B*). Both recombinant spike protein RBD and ectodomain (SΔTM) were produced using a mammalian expression system that retained proper protein glycosylation equivalent to that observed during virus replication (Figs. 1*C* and S1*A*). Mice were immunized with these recombinant spike proteins to generate antibodies against the SARS-CoV-2 virus, followed by cell fusion to generate a hybridoma-producing antibody. Culture supernatants were prescreened by enzyme-linked immunosorbent assay (ELISA), WB, and immunoprecipitation (IP), and six monoclonal hybridomas were isolated and evaluated.

To characterize these antibodies in detail, they were first purified from the culture supernatant and examined in terms of ELISA and WB performance. Four monoclonal antibodies derived from the antigen produced by *E. coli* (Clones R15, R22, R31, and R52) and two from mammalian cells (S1D7 and S3D8) showed remarkable performance. In the ELISA binding assay, all six clones bound glycosylated RBD with high affinity. When tested against spike glycoprotein (SΔTM), two clones (R15 and R52) could not be distinguished from nonimmune IgG (Fig. 1*D*). We noted that IgG2 subclass members tended to have higher binding affinities. Half maximal effective concentration (EC_{50}) required for these antibodies to bind RBD and SΔTM glycoproteins falls at the low hundreds ng/ml (Fig. 1*E*). In WB, where target proteins are reduced and denatured, all clones established by *E. coli* produced-antigens performed well at detecting RBD and SΔTM proteins regardless of glycosylation (Fig. 1*F*, left, and Figs. 1*G* and S1*B*). Among them, clones R15 and R52 showed higher sensitivity in WB. In addition, R52 was capable of detecting not only artificial spike glycoprotein carrying T4 foldon, but also native spike glycoprotein expressed in 293T cells on WB (Fig. 1*H*). However, neither RBD nor SΔTM could be detected by antibody clones established by the mammalian antigen (S1D7 and S3D8) on WB, suggesting a strong preference for intact tertiary structure (Fig. 1*F*, right, see also Fig. S3, *B–D*).

S1D7 and S3D8 antibodies showed higher performance on IP and IF

An antibody capable of recognizing the intact tertiary structure of spike proteins would contribute to research dissecting the molecular mechanism of SARS-CoV-2 infection, especially cell entry, where these proteins play a significant role. The IP activity of antibodies can be correlated with the activity of capturing the native structure of the target protein and neutralizing the infection. We examined the IP performance of our monoclonal antibodies. Although all clones were capable of immunoprecipitating RBD and SΔTM glycoproteins, clones R22, R31, S1D7, and S3D8 demonstrated superior IP efficiency for SΔTM, whereas R22, S1D7, and S3D8 showed higher IP efficiency for RBD glycoprotein (Figs. 2*A* and S2*A*). As shown in Figure 2*B*, our antibodies recognize the spike protein in a glycosylation-independent manner, and the IP efficiencies of R22, R31, S1D7, and S3D8, although mild, outperformed others. Noticeably, although clones S1D7 and S3D8 are not capable of performing WB (Fig. 1*F*), a strong preference for tertiary structure grants them remarkable performance in IP, where RBD and SΔTM glycoproteins were pulled down in their native conformation. Of note, we found that S1D7 and S3D8 could maintain intact IP efficiency under highly stringent experimental conditions where sodium dodecyl sulfate (SDS) was present (Fig. S2*B*).

Next, we examined whether our antibodies could be used in the immunofluorescence assay (IF). An antibody applicable for IP would also have activity in IF. Cellular localization of spike proteins is essential for elucidating the mechanism of packaging and maturation of virions during release from the cellular membrane. We tested our antibodies' performance in IF using HeLa cells overexpressing spike protein with the transmembrane domain. Consistent with their performance in the above-mentioned assays (Fig. 2, *A* and *B*), both S1D7 and S3D8 could detect spike proteins expressed homogeneously on the apical side of HeLa cells with a high signal-to-noise ratio

Clone S1D7 and S3D7 could not detect either SΔTM or RBD in WB. *G*, detection of nonglycosylated SΔTM using established monoclonal antibodies. Four clones could detect SΔTM (30 ng per lane), regardless of glycosylation. *H*, detection of spike proteins expressed in 293T cells. Lysates of 293T cells expressing artificial spikes carrying T4 foldon or wild-type spike glycoproteins were separated by SDS-PAGE, followed by WB using antibody R52. Foldon, T4 fabritin trimerization motif; GST, glutathione S-transferase; MBP, maltose-binding protein; n.i., nonimmune mouse IgG; NTD, N-terminal domain; RBD, receptor-binding domain; SΔTM, spike lacking TM domain; SBP, streptavidin-binding peptide; SS, signal peptide; TM, transmembrane domain.

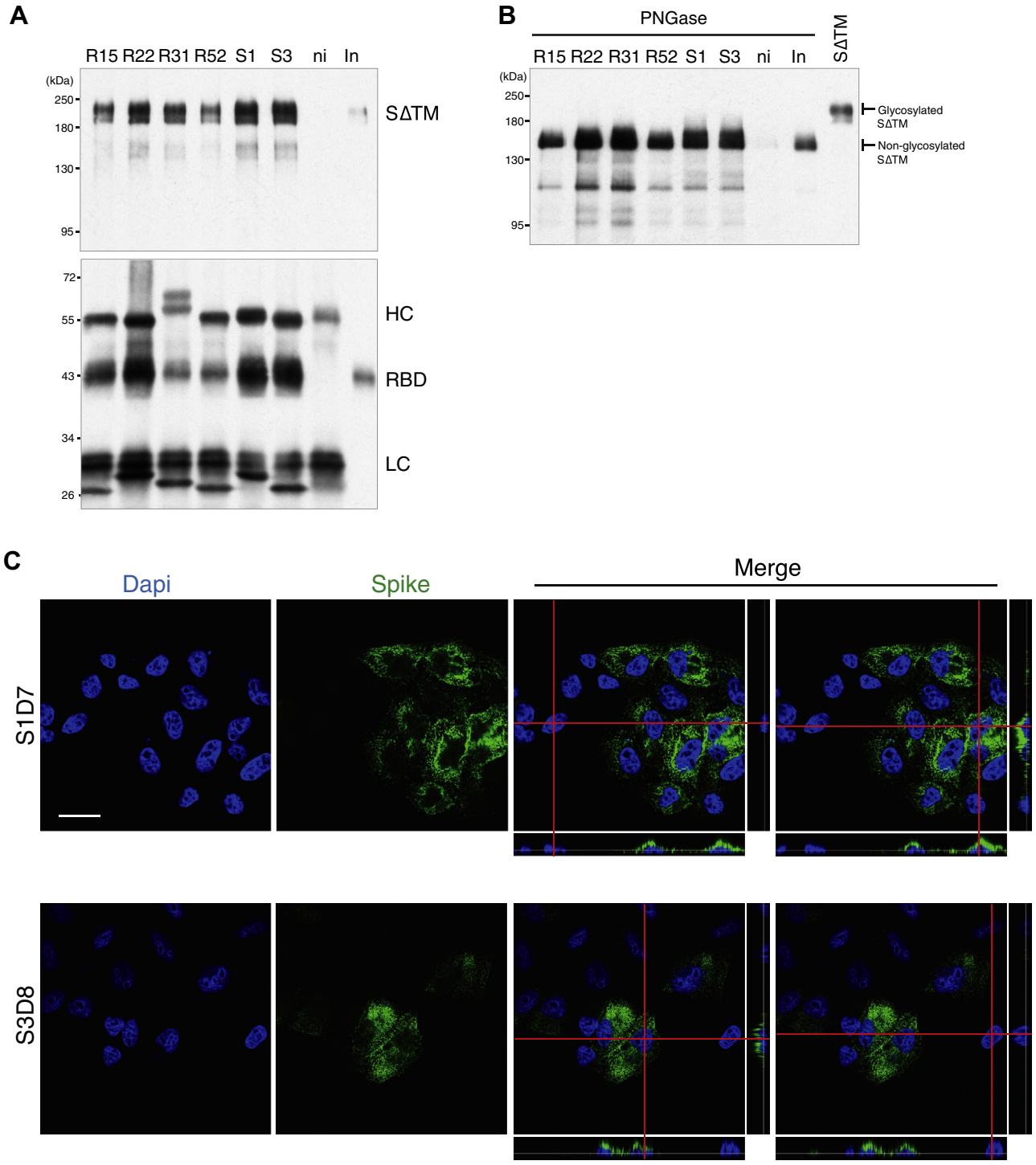

Figure 2. Application for immunoprecipitation and immunofluorescence. *A*, immunoprecipitation (IP) of trimeric glycosylated spike protein (SΔTM) using established monoclonal antibodies. All clones were capable of pulling down RBD and spike glycoprotein. Higher IP efficiency of spike glycoprotein was observed in clones R22, R31, S1D7, and S3D8. For RBD glycoprotein, clone R22, S1D7, and S3D8 showed higher IP efficiency. *B*, IP of trimeric spike protein deglycosylated by PNGase F using established monoclonal antibodies. "SΔTM" indicates SΔTM glycoprotein untreated with PNGase F. All clones are capable of pulling down deglycosylated spike protein. Higher IP efficiency was observed in clones R22, R31, S1D7, and S3D8. *C*, immunofluorescence (IF) staining of spike glycoprotein expressed in HeLa cells with monoclonal antibodies S1D7 and S3D8. Spike protein localized on the apical surface of transfected HeLa cells. Scale bar, 30 μm. HC, IgG heavy chain; In, input; LC, IgG light chain; ni, nonimmune mouse IgG; SΔTM, trimeric spike protein without transmembrane domain; S1, S1D7; S3, S3D8.

(Figs. 2*C* and S2*C*). However, their localization pattern is different from that observed for SARS-CoV-1 spike proteins, which are exclusively localized in the Golgi during infection (39) (see also Fig. 4*B*). Mouse hepatitis coronavirus spike protein localizes in the endoplasmic reticulum–Golgi intermediate compartment (ERGIC) in a membrane (M) protein-dependent manner (40). We then examined the effect of M protein on cellular localization of spike proteins. As shown in

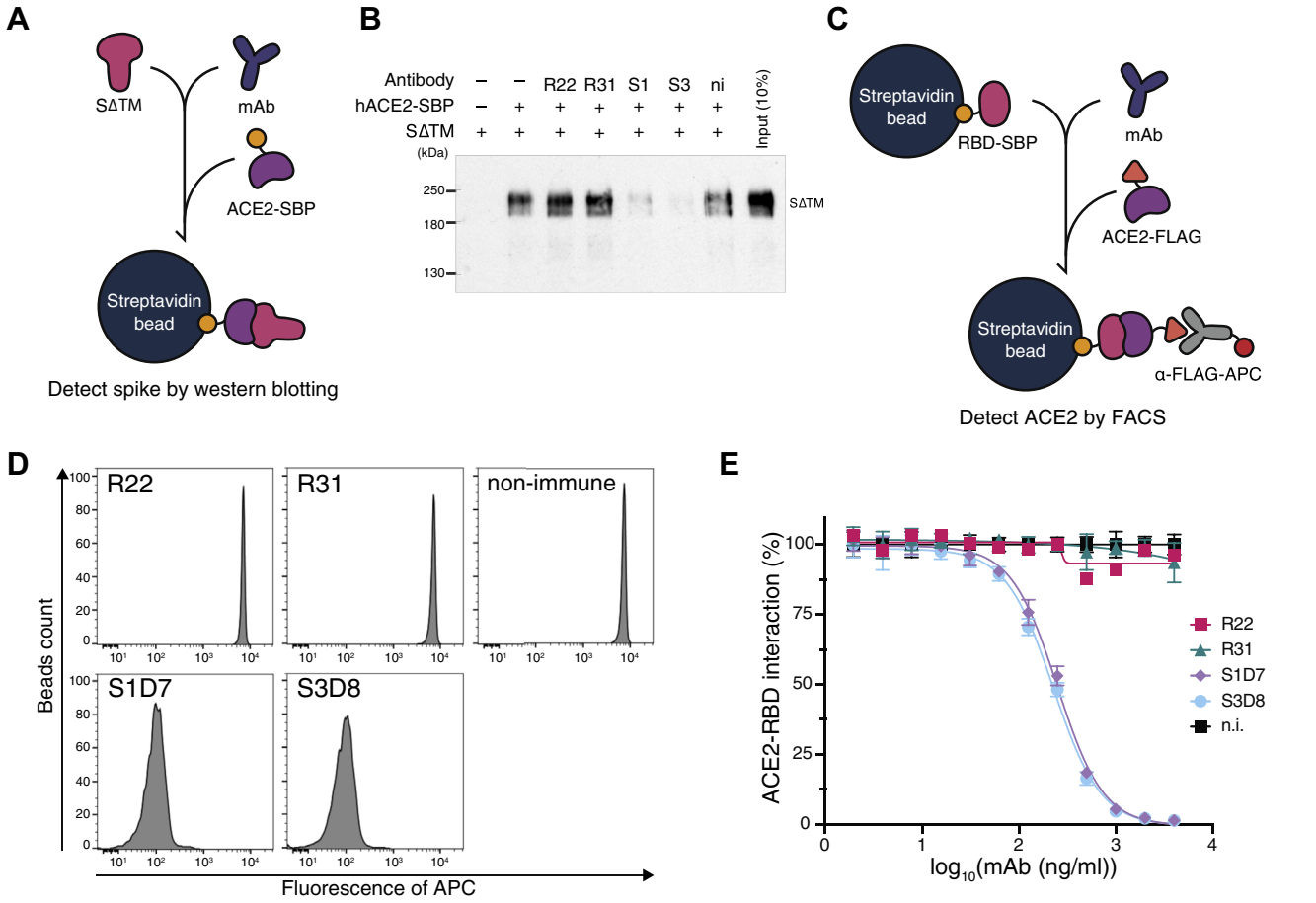

Figure 3. Inhibition of ACE2–spike interaction by S1D7 and S3D8. *A*, a schematic of the spike pull-down assay designed to evaluate inhibition of ACE2–spike binding by monoclonal antibody. Spike glycoprotein lacking TM domain (SΔTM) was mixed with a monoclonal antibody. ACE2-SBP was applied to capture SΔTM onto streptavidin beads competitively. Captured SΔTM was detected by WB as a measurement of the antibody's inhibitory ability. *B*, WB of spike pull-down assay using antibody R52. In the presence of clones S1D7 and S3D8, ACE2 was not able to pull down SΔTM. *C*, schematic of bead-based neutralization assay designed to quantify inhibition of ACE2–RBD binding by monoclonal antibody. RBD-SBP glycoprotein immobilized on streptavidin beads was mixed with a monoclonal antibody. ACE2-FLAG was applied to bind competitively with RBD. ACE2–RBD binding was quantified by measuring the signal given by an anti-FLAG antibody conjugated with APC fluorophore using FACS. *D*, one set of representative FACS results of a bead-based neutralization assay in the presence of 4 μg/ml monoclonal antibodies. Clones S1D7 and S3D8 significantly inhibited ACE2-RBD interaction, shown as lowered fluorescence intensity of APC. *E*, binding profiles of potent neutralizing antibodies. Error bars indicate standard deviation (n = 3). Clones R22 and R31 showed no inhibition of ACE2-RBD binding, while S1D7 and S3D8 inhibited ACE2-RBD interaction at lower ng/ml levels. ni, nonimmune mouse IgG; S1, S1D7; S3, S3D8.

Figure S2, *D* and *E*, M protein did not appear to have any impact on localization of spike proteins in HeLa cells, suggesting that mechanisms of viral assembly in SARS-CoV-2 are different from that of SARS-CoV-1 and mouse hepatitis coronavirus.

ACE2–spike binding inhibition of the monoclonal antibodies

The manner in which antibodies bind and pull down spike glycoproteins in an IP experiment resembles the process of antibody-mediated neutralization, where spike–ACE2 interaction is intercepted by competitive binding between neutralizing antibodies and spike glycoprotein. We then examined whether they were capable of inhibiting spike–ACE2 binding or even neutralizing SARS-CoV-2 infection. First, we performed a spike pull-down assay in which the spike glycoprotein was pulled down by ACE2 in the presence of monoclonal antibodies (Fig. 3*A* and S3*A*). Clones S1D7 and S3D8 clearly inhibited spike–ACE2 binding, as shown by the dimmed spike signal in WB (Fig. 3*B*). To quantify the inhibition ability, we performed a bead-based neutralization assay by measuring the amount of ACE2 bound to RBD beads after blocking with monoclonal antibodies (Fig. 3*C*). Antibodies R22 and R31 showed no disruption of ACE2–RBD interaction, whereas S1D7 and S3D8 showed robust hindrance of ACE2–RBD binding with IC_{50} values of 248.2 ng/ml and 225.6 ng/ml, respectively (Fig. 3, *D* and *E*). S1D7 and S3D8's abilities to inhibit spike–ACE2 binding was consistent with their superior performance in IP experiments. Four monoclonal antibodies derived from the antigen produced by *E. coli* (Clones R15, R22, R31, and R52) were found to recognize continuous epitope 549-TGVLTESNKKFLPFQQFGRD-568 of spike protein RBD (Fig. S3, *B–D*). In contrast, an epitope of two antibodies from mammalian cells (S1D7 and S3D8) could not be determined (Fig. S3, *B–D*). The fact that they fail to recognize segmented RBD suggests that they recognize an intact tertiary structure of the spike protein.

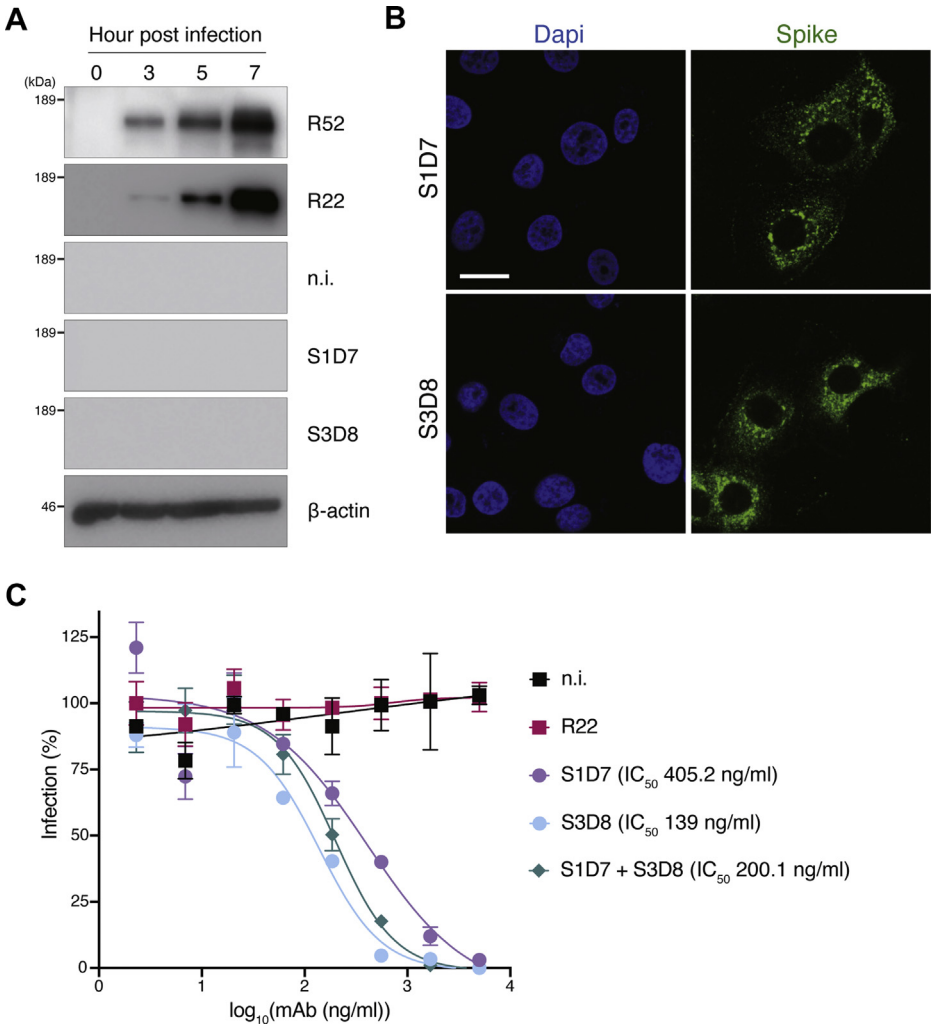

Figure 4. S1D7 and S3D8 neutralized SARS-CoV-2 infection. *A*, Spike glycoprotein was expressed in VeroE6/TM2 cells during SARS-CoV-2 infection. Spike glycoproteins were detected by western blots using anti-spike antibodies R22 and R52. *B*, immunofluorescence staining of spike glycoprotein expressed in VeroE6/TM2 cells infected with SARS-CoV-2 at 7 h postinfection. Scale bar, 20 μm. *C*, S1D7 and S3D8 are capable of neutralizing live virus infections. Although clone R22 failed to protect VeroE6/TM2 cells from SARS-CoV-2 infection, S1D7 and S3D8 blocked SARS-CoV-2 infection significantly with IC_{50} values of 405.2 ng/ml and 139 ng/ml, respectively. S1D7 and S3D8 cocktail showed intermediate neutralizing activity (200.1 ng/ml). Error bars indicate standard deviation (n = 3).

S1D7 and S3D8 showed neutralizing activity against SARS-CoV-2

Next, we asked whether our antibodies inhibit SARS-CoV-2 infection in VeroE6/TMPRSS2 (TM2) cells, which is susceptible to SARS-CoV-2 infection compared with the parental VeroE6 cell line by expressing TMPRSS2 (41). In WB, antibodies R52 and R22, but not S1D7 and S3D8, could detect spike glycoprotein along with the progression of SARS-CoV-2 infection in VeroE6/TM2 cells (Fig. 4*A*). On the other hand, S1D7 and S3D8 were applicable to IF in infected VeroE6/TM2 cells. Spike showed a punctate distribution pattern in the perinuclear region resembling ER and ERGIC (42) (Fig. 4*B*). The subcellular localization of spike resembled that of the N protein in Vero cells infected with SARS-CoV-1 (39), suggesting assembly of SARS-CoV-2 virion in the cytoplasm. We then conducted a live virus neutralization assay to examine whether clones S1D7 and S3D8 inhibit the live virus infection. As expected, although clone R22 failed to protect VeroE6/TM2 from SARS-CoV-2 infection, S1D7 and S3D8 blocked SARS-CoV-2 infection significantly with IC_{50} values of 405.2 ng/ml and 139 ng/ml, respectively, even at relatively high titers of 1500 $TCID_{50}$ (Fig. 4*C* and Table S1). A cocktail of S1D7 and S3D8 showed intermediate neutralizing activity (200.1 ng/ml), suggesting that S1D7 and S3D8 share an inhibitory mechanism.

Recombinant human/mouse chimeric antibodies R52h and S1D7h are applicable for WB and IF, respectively

Our mouse antibodies would not be applicable for use in clinical treatment, if not chimeric and humanized, due to their immunogenicity (30, 43). In the hope of applying the antibodies of clinical settings, the variable regions of the antibodies were determined (Table S2), followed by the production of recombinant antibodies based on plasmid transfection to Expi293 or 293T cell lines. We selected three antibodies from among these and generated humanized chimeric antibodies

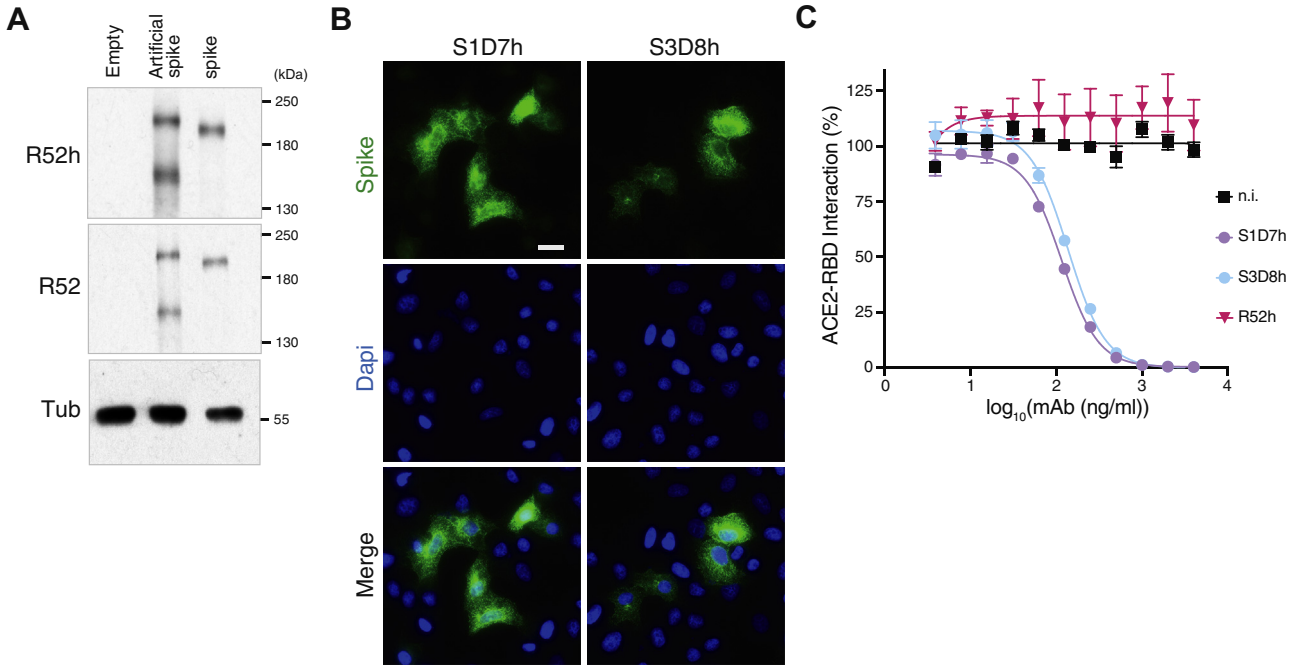

Figure 5. Recombinant human/mouse chimeric antibodies R52h, S1D7h, and S3D8h. *A*, R52h is applicable for WB. Lysates of 293T cells expressing artificial spikes carrying T4 foldon or wild-type spike glycoproteins were separated by SDS-PAGE, followed by WB using human/mouse chimeric antibody R52h, which was secreted by Expi293F cells. *B*, S1D7h and S3D8h are applicable for IF. Spike glycoprotein expressed in HeLa cells was stained with human/mouse chimeric antibodies S1D7h or S3D8h, which were secreted by Expi293F cells. Scale bar, 20 μm. *C*, Binding profiles of potent neutralizing antibodies. ni, nonimmune mouse IgG. Error bars indicate standard deviation (n = 3).

designated as R52h, S1D7h, and S3D8h by fusing them with the constant region of human IgG1κ for R52, S1D7, and S3D8. R52h was capable of detecting artificial spike glycoprotein carrying T4 foldon, and native spike glycoprotein expressed in 293T cells on WB as well as R52 (Figs. 5*A* and S4*A*). In IF, S1D7h could detect spike proteins expressed in HeLa cells (Figs. 5*B* and S4*B*). Notably, S1D7h and S3D8h showed robust hindrance of ACE2–RBD binding with IC_{50} values of 116.3 ng/ml and 137.2 ng/ml, respectively (Fig. 5*C*).

Discussion

Emerging SARS-CoV-2 is a global public health threat to society, which is predicted to be long-term for several years (44). Although there are multiple ongoing endeavors to develop neutralizing antibodies, vaccines, and drugs against the virus (45, 46), the lack of adequate, licensed countermeasures underscores the need for a more detailed and comprehensive understanding of the molecular mechanisms underlying the pathogenesis of the virus (47). Fundamental knowledge has significant implications for developing countermeasures against the virus, including diagnosis, vaccine design, and drug discovery. Due to the above reasons, and our experiences with routine antibody productions (48, 49), we have established and characterized mouse monoclonal antibodies that can be used to dissect the molecular mechanism of the virus life cycle. These antibodies would serve as a reliable toolset for basic research investigating the expression profile and subcellular localization of spike glycoprotein during viral entry, replication, packaging, and budding. These antibodies could help to identify novel host factors interacting with spike glycoprotein when used in IP in combination with mass spectrometry. Therefore, advancement in basic research would accelerate the discovery of drugs targeting virus transmission.

Our antibodies, S1D7 and S3D8, have been shown to attenuate the interaction of spike proteins with ACE2 and neutralize infection of VeroE6/TM2 cells by SARS-CoV-2. It is worth noting that although their neutralizing activities (IC_{50} of 405.2 ng/ml and 139 ng/ml) appeared to be lower than those of human antibodies reported previously (Fig. 4*C* and Table S1), the stringency of experimental conditions (relatively high virus titer of 1500 $TCID_{50}$) tend to underestimate neutralizing activities of our antibodies compared with other research groups. Specifically, we used a high multiplicity of live SARS-CoV-2 virus to infect VeroE6/TM2 cells, which are more prone to virus infection than the commonly adopted VeroE6 cell line. Therefore, it is difficult to compare antibody efficacy among them (50). In addition to *in vitro* infection, their neutralizing activity *in vivo* should be examined in animal models that recapitulate SARS-CoV-2 disease. They may be valuable for investigating the mechanism of immune responses to the virus during passive immunization using mouse models for SARS-CoV-2 infection (28, 51–55). They could show stable performance due to lot-to-lot consistency and act as benchmarks for other antibodies and drug developments.

Experimental procedures

Experimental procedures are provided as supporting information.

Data availability

All data are contained within the article.

Supporting information—This article contains supporting information (56, 57).

Acknowledgments—We thank A. Ishida, M. Kobayashi, and Y. Kurihara for technical assistance and advice on the production of antibodies.

Author contributions—Y. G., H. S., and K. M. conceived the project, designed the experiments, and wrote the article. Y. G., A. K., M. T., and K. M. performed the experiments. All the authors analyzed the data and contributed to the preparation of the article.

Funding and additional information—This work was supported by the Keio University Global Research Institute (KGRI) COVID-19 Pandemic Crisis Research Grant (to M. T., H. S., and K. M.) and the Keio Donner Project, which is devoted to Shibasaburo Kitasato, the founder of Keio University School of Medicine. This study was also supported in part by AMED (JP18fk0108076 to A. K.), NOMURA Microbial Community Control Project in ERATO of the Japan Science and Technology Agency (to A. K.), and Research Support Program to Tackle COVID-19 Related Emergency Problems, University of Tsukuba (to A. K.).

Conflict of interest—The authors declare that they have no conflicts of interest with the contents of this article.

Abbreviations—The abbreviations used are: ACE2, angiotensin-converting enzyme 2; COVID-19, coronavirus disease 2019; ELISA, enzyme-linked immunosorbent assay; ERGIC, endoplasmic reticulum–Golgi intermediate compartment; IF, immunofluorescence; IP, immunoprecipitatio; RBD, receptor-binding domain; RSV, respiratory syncytial virus; SARS-CoV-2, severe acute respiratory syndrome coronavirus 2; SDS, sodium dodecyl sulfate; WB, western blotting.

References

1. Li, Q., Guan, X., Wu, P., Wang, X., Zhou, L., Tong, Y., Ren, R., Leung, K. S. M., Lau, E. H. Y., Wong, J. Y., Xing, X., Xiang, N., Wu, Y., Li, C., Chen, Q., *et al.* (2020) Early transmission dynamics in Wuhan, China, of novel coronavirus-infected pneumonia. *N. Engl. J. Med.* **382**, 1199–1207
2. Huang, C., Wang, Y., Li, X., Ren, L., Zhao, J., Hu, Y., Zhang, L., Fan, G., Xu, J., Gu, X., Cheng, Z., Yu, T., Xia, J., Wei, Y., Wu, W., *et al.* (2020) Clinical features of patients infected with 2019 novel coronavirus in Wuhan, China. *Lancet* **395**, 497–506
3. Walker, L. M., and Burton, D. R. (2018) Passive immunotherapy of viral infections: 'super-antibodies' enter the fray. *Nat. Rev. Immunol.* **18**, 297–308
4. Klasse, P. J., and Moore, J. P. (2020) Antibodies to SARS-CoV-2 and their potential for therapeutic passive immunization. *Elife* **9**, 1–11
5. Graham, B. S., and Ambrosino, D. M. (2015) History of passive antibody administration for prevention and treatment of infectious diseases. *Curr. Opin. HIV AIDS* **10**, 129–134
6. Connor, E. M. (1999) Palivizumab, a humanized respiratory syncytial virus monoclonal antibody, reduces hospitalization from respiratory syncytial virus infection in hieh-risk infants. The IMpact-RSV study group. *Radiology* **210**, 295–296
7. Caskey, M., Klein, F., and Nussenzweig, M. C. (2019) Broadly neutralizing anti-HIV-1 monoclonal antibodies in the clinic. *Nat. Med.* **25**, 547–553
8. Corti, D., Passini, N., Lanzavecchia, A., and Zambon, M. (2016) Rapid generation of a human monoclonal antibody to combat Middle East respiratory syndrome. *J. Infect. Public Health* **9**, 231–235
9. Corti, D., Misasi, J., Mulangu, S., Stanley, D. A., Kanekiyo, M., Wollen, S., Ploquin, A., Doria-Rose, N. A., Staupe, R. P., Bailey, M., Shi, W., Choe, M., Marcus, H., Thompson, E. A., Cagigi, A., *et al.* (2016) Protective monotherapy against lethal Ebola virus infection by a potently neutralizing antibody. *Science* **351**, 1339–1342
10. Corti, D., Cameroni, E., Guarino, B., Kallewaard, N. L., Zhu, Q., and Lanzavecchia, A. (2017) Tackling influenza with broadly neutralizing antibodies. *Curr. Opin. Virol.* **24**, 60–69
11. Dhama, K., Sharun, K., Tiwari, R., Dadar, M., Malik, Y. S., Singh, K. P., and Chaicumpa, W. (2020) COVID-19, an emerging coronavirus infection: Advances and prospects in designing and developing vaccines, immunotherapeutics, and therapeutics. *Hum. Vaccin. Immunother.* **16**, 1232–1238
12. Jawhara, S. (2020) Could intravenous immunoglobulin collected from recovered coronavirus patients protect against COVID-19 and strengthen the immune system of new patients? *Int. J. Mol. Sci.* **21**, 2272
13. Jiang, S., Hillyer, C., and Du, L. (2020) Neutralizing antibodies against SARS-CoV-2 and other human coronaviruses. *Trends Immunol.* **41**, 355–359
14. Ni, L., Ye, F., Cheng, M. L., Feng, Y., Deng, Y. Q., Zhao, H., Wei, P., Ge, J., Gou, M., Li, X., Sun, L., Cao, T., Wang, P., Zhou, C., Zhang, R., *et al.* (2020) Detection of SARS-CoV-2-specific humoral and cellular immunity in COVID-19 convalescent individuals. *Immunity* **52**, 971–977.e973
15. Robbiani, D. F., Gaebler, C., Muecksch, F., Lorenzi, J. C. C., Wang, Z., Cho, A., Agudelo, M., Barnes, C. O., Gazumyan, A., Finkin, S., Hagglof, T., Oliveira, T. Y., Viant, C., Hurley, A., Hoffmann, H. H., *et al.* (2020) Convergent antibody responses to SARS-CoV-2 in convalescent individuals. *Nature* **584**, 437–442
16. Liu, L., Wang, P., Nair, M. S., Yu, J., Rapp, M., Wang, Q., Luo, Y., Chan, J. F., Sahi, V., Figueroa, A., Guo, X. V., Cerutti, G., Bimela, J., Gorman, J., Zhou, T., *et al.* (2020) Potent neutralizing antibodies against multiple epitopes on SARS-CoV-2 spike. *Nature* **584**, 450–456
17. Cao, Y., Su, B., Guo, X., Sun, W., Deng, Y., Bao, L., Zhu, Q., Zhang, X., Zheng, Y., Geng, C., Chai, X., He, R., Li, X., Lv, Q., Zhu, H., *et al.* (2020) Potent neutralizing antibodies against SARS-CoV-2 identified by high-throughput single-cell sequencing of convalescent patients' B cells. *Cell* **182**, 73–84.e16
18. Chen, X., Li, R., Pan, Z., Qian, C., Yang, Y., You, R., Zhao, J., Liu, P., Gao, L., Li, Z., Huang, Q., Xu, L., Tang, J., Tian, Q., Yao, W., *et al.* (2020) Human monoclonal antibodies block the binding of SARS-CoV-2 spike protein to angiotensin converting enzyme 2 receptor. *Cell Mol. Immunol.* **17**, 647–649
19. Chi, X., Yan, R., Zhang, J., Zhang, G., Zhang, Y., Hao, M., Zhang, Z., Fan, P., Dong, Y., Yang, Y., Chen, Z., Guo, Y., Zhang, J., Li, Y., Song, X., *et al.* (2020) A neutralizing human antibody binds to the N-terminal domain of the Spike protein of SARS-CoV-2. *Science* **655**, eabc6952
20. Wang, C., Li, W., Drabek, D., Okba, N. M. A., van Haperen, R., Osterhaus, A. D. M. E., van Kuppeveld, F. J. M., Haagmans, B. L., Grosveld, F., and Bosch, B. J. (2020) A human monoclonal antibody blocking SARS-CoV-2 infection. *Nat. Commun.* **11**, 1–6
21. Wu, Y., Wang, F., Shen, C., Peng, W., Li, D., Zhao, C., Li, Z., Li, S., Bi, Y., Yang, Y., Gong, Y., Xiao, H., Fan, Z., Tan, S., Wu, G., *et al.* (2020) A noncompeting pair of human neutralizing antibodies block COVID-19 virus binding to its receptor ACE2. *Science* **368**, 1274–1278
22. Ju, B., Zhang, Q., Ge, J., Wang, R., Sun, J., Ge, X., Yu, J., Shan, S., Zhou, B., Song, S., Tang, X., Yu, J., Lan, J., Yuan, J., Wang, H., *et al.* (2020) Human neutralizing antibodies elicited by SARS-CoV-2 infection. *Nature* **584**, 115–119
23. Zeng, X., Li, L., Lin, J., Li, X., Liu, B., Kong, Y., Zeng, S., Du, J., Xiao, H., Zhang, T., Zhang, S., and Liu, J. (2020) Isolation of a human monoclonal antibody specific for the receptor binding domain of SARS-CoV-2 using a competitive phage biopanning strategy. *Antibody Ther.* **3**, 95–100
24. Wan, J., Xing, S., Ding, L., Wang, Y., Gu, C., Wu, Y., Rong, B., Li, C., Wang, S., Chen, K., He, C., Zhu, D., Yuan, S., Qiu, C., Zhao, C., *et al.*

(2020) Human-IgG-neutralizing monoclonal antibodies block the SARS-CoV-2 infection. *Cell Rep.* **32**, 107918
25. Shi, R., Shan, C., Duan, X., Chen, Z., Liu, P., Song, J., Song, T., Bi, X., Han, C., Wu, L., Gao, G., Hu, X., Zhang, Y., Tong, Z., Huang, W., *et al.* (2020) A human neutralizing antibody targets the receptor-binding site of SARS-CoV-2. *Nature* **584**, 120–124
26. Pinto, D., Park, Y. J., Beltramello, M., Walls, A. C., Tortorici, M. A., Bianchi, S., Jaconi, S., Culap, K., Zatta, F., De Marco, A., Peter, A., Guarino, B., Spreafico, R., Cameroni, E., Case, J. B., *et al.* (2020) Cross-neutralization of SARS-CoV-2 by a human monoclonal SARS-CoV antibody. *Nature* **583**, 290–295
27. Rogers, T. F., Zhao, F., Huang, D., Beutler, N., Burns, A., He, W.-t., Limbo, O., Smith, C., Song, G., Woehl, J., Yang, L., Abbott, R. K., Callaghan, S., Garcia, E., Hurtado, J., *et al.* (2020) Isolation of potent SARS-CoV-2 neutralizing antibodies and protection from disease in a small animal model. *Science* **7520**, eabc7520
28. Hassan, A. O., Case, J. B., Winkler, E. S., Thackray, L. B., Kafai, N. M., Bailey, A. L., McCune, B. T., Fox, J. M., Chen, R. E., Alsoussi, W. B., Turner, J. S., Schmitz, A. J., Lei, T., Shrihari, S., Keeler, S. P., *et al.* (2020) A SARS-CoV-2 infection model in mice demonstrates protection by neutralizing antibodies. *Cell* **182**, 744–753.e744
29. Zost, S. J., Gilchuk, P., Case, J. B., Binshtein, E., Chen, R. E., Nkolola, J. P., Schafer, A., Reidy, J. X., Trivette, A., Nargi, R. S., Sutton, R. E., Suryadevara, N., Martinez, D. R., Williamson, L. E., Chen, E. C., *et al.* (2020) Potently neutralizing and protective human antibodies against SARS-CoV-2. *Nature* **584**, 443–449
30. Hansel, T. T., Kropshofer, H., Singer, T., Mitchell, J. A., and George, A. J. (2010) The safety and side effects of monoclonal antibodies. *Nat. Rev. Drug Discov.* **9**, 325–338
31. Cohen, J. (2020) The race is on for antibodies that stop the new coronavirus. *Science* **368**, 564–565
32. Hoffmann, M., Kleine-Weber, H., Schroeder, S., Krüger, N., Herrler, T., Erichsen, S., Schiergens, T. S., Herrler, G., Wu, N. H., Nitsche, A., Müller, M. A., Drosten, C., and Pöhlmann, S. (2020) SARS-CoV-2 cell entry depends on ACE2 and TMPRSS2 and is blocked by a clinically proven protease inhibitor. *Cell* **181**, 271–280.e278
33. Song, W., Gui, M., Wang, X., and Xiang, Y. (2018) Cryo-EM structure of the SARS coronavirus spike glycoprotein in complex with its host cell receptor ACE2. *Plos Pathog.* **14**, e1007236
34. Ou, X., Liu, Y., Lei, X., Li, P., Mi, D., Ren, L., Guo, L., Guo, R., Chen, T., Hu, J., Xiang, Z., Mu, Z., Chen, X., Chen, J., Hu, K., *et al.* (2020) Characterization of spike glycoprotein of SARS-CoV-2 on virus entry and its immune cross-reactivity with SARS-CoV. *Nat. Commun.Cell* **11**, 1620
35. Walls, A. C., Park, Y. J., Tortorici, M. A., Wall, A., McGuire, A. T., and Veesler, D. (2020) Structure, function, and antigenicity of the SARS-CoV-2 spike glycoprotein. *Cell* **181**, 281–292.e286
36. Tai, W., Zhang, X., He, Y., Jiang, S., and Du, L. (2020) Identification of SARS-CoV RBD-targeting monoclonal antibodies with cross-reactive or neutralizing activity against SARS-CoV-2. *Antiviral Res.* **179**, 104820
37. Wrapp, D., Wang, N., Corbett, K. S., Goldsmith, J. A., Hsieh, C. L., Abiona, O., Graham, B. S., and McLellan, J. S. (2020) Cryo-EM structure of the 2019-nCoV spike in the prefusion conformation. *Science* **367**, 1260–1263
38. Miroshnikov, K. A., Marusich, E. I., Cerritelli, M. E., Cheng, N., Hyde, C. C., Steven, A. C., and Mesyanzhinov, V. V. (1998) Engineering trimeric fibrous proteins based on bacteriophage T4 adhesins. *Protein Eng.* **11**, 329–332
39. Stertz, S., Reichelt, M., Spiegel, M., Kuri, T., Martinez-Sobrido, L., Garcia-Sastre, A., Weber, F., and Kochs, G. (2007) The intracellular sites of early replication and budding of SARS-coronavirus. *Virology* **361**, 304–315
40. Opstelten, D. J., Raamsman, M. J., Wolfs, K., Horzinek, M. C., and Rottier, P. J. (1995) Envelope glycoprotein interactions in coronavirus assembly. *J. Cell Biol* **131**, 339–349
41. Matsuyama, S., Nao, N., Shirato, K., Kawase, M., Saito, S., Takayama, I., Nagata, N., Sekizuka, T., Katoh, H., Kato, F., Sakata, M., Tahara, M., Kutsuna, S., Ohmagari, N., Kuroda, M., *et al.* (2020) Enhanced isolation of SARS-CoV-2 by TMPRSS2- expressing cells. *Proc. Natl. Acad. Sci. U. S. A.* **117**, 7001–7003
42. Sadasivan, J., Singh, M., and Sarma, J. D. (2017) Cytoplasmic tail of coronavirus spike protein has intracellular targeting signals. *J. Biosci.* **42**, 231–244
43. Reichert, J. M., Rosensweig, C. J., Faden, L. B., and Dewitz, M. C. (2005) Monoclonal antibody successes in the clinic. *Nat. Biotechnol.* **23**, 1073–1078
44. Kissler, S. M., Tedijanto, C., Goldstein, E., Grad, Y. H., and Lipsitch, M. (2020) Projecting the transmission dynamics of SARS-CoV-2 through the postpandemic period. *Science* **368**, 860–868
45. Callaway, E. (2020) The race for coronavirus vaccines: A graphical guide. *Nature* **580**, 576–577
46. Riva, L., Yuan, S., Yin, X., Martin-Sancho, L., Matsunaga, N., Pache, L., Burgstaller-Muehlbacher, S., De Jesus, P. D., Teriete, P., Hull, M. V., Chang, M. W., Chan, J. F., Cao, J., Poon, V. K., Herbert, K. M., *et al.* (2020) Discovery of SARS-CoV-2 antiviral drugs through large-scale compound repurposing. *Nature* **586**, 113–119
47. Artika, I. M., Dewantari, A. K., and Wiyatno, A. (2020) Molecular biology of coronaviruses: Current knowledge. *Heliyon* **6**, e04743
48. Iwasaki, Y. W., Murano, K., Ishizu, H., Shibuya, A., Iyoda, Y., Siomi, M. C., Siomi, H., and Saito, K. (2016) Piwi modulates chromatin accessibility by regulating multiple factors including histone H1 to repress transposons. *Mol. Cell* **63**, 408–419
49. Murano, K., Iwasaki, Y. W., Ishizu, H., Mashiko, A., Shibuya, A., Kondo, S., Adachi, S., Suzuki, S., Saito, K., Natsume, T., Siomi, M. C., and Siomi, H. (2019) Nuclear RNA export factor variant initiates piRNA-guided co-transcriptional silencing. *EMBO J.* **38**, e102870
50. Tse, L. V., Meganck, R. M., Graham, R. L., and Baric, R. S. (2020) The current and future state of vaccines, antivirals and gene therapies against emerging coronaviruses. *Front. Microbiol.* **11**, 658
51. Bao, L., Deng, W., Huang, B., Gao, H., Liu, J., Ren, L., Wei, Q., Yu, P., Xu, Y., Qi, F., Qu, Y., Li, F., Lv, Q., Wang, W., Xue, J., *et al.* (2020) The pathogenicity of SARS-CoV-2 in hACE2 transgenic mice. *Nature* **583**, 830–833
52. Jiang, R. D., Liu, M. Q., Chen, Y., Shan, C., Zhou, Y. W., Shen, X. R., Li, Q., Zhang, L., Zhu, Y., Si, H. R., Wang, Q., Min, J., Wang, X., Zhang, W., Li, B., *et al.* (2020) Pathogenesis of SARS-CoV-2 in transgenic mice expressing human angiotensin-converting enzyme 2. *Cell* **182**, 50–58.e58
53. Dinnon, K. H., 3rd, Leist, S. R., Schafer, A., Edwards, C. E., Martinez, D. R., Montgomery, S. A., West, A., Yount, B. L., Jr., Hou, Y. J., Adams, L. E., Gully, K. L., Brown, A. J., Huang, E., Bryant, M. D., Choong, I. C., *et al.* (2020) A mouse-adapted model of SARS-CoV-2 to test COVID-19 countermeasures. *Nature* **586**, 560–566
54. Winkler, E. S., Bailey, A. L., Kafai, N. M., Nair, S., McCune, B. T., Yu, J., Fox, J. M., Chen, R. E., Earnest, J. T., Keeler, S. P., Ritter, J. H., Kang, L. I., Dort, S., Robichaud, A., Head, R., *et al.* (2020) SARS-CoV-2 infection of human ACE2-transgenic mice causes severe lung inflammation and impaired function. *Nat. Immunol.* **21**, 1327–1335
55. Israelow, B., Song, E., Mao, T., Lu, P., Meir, A., Liu, F., Alfajaro, M. M., Wei, J., Dong, H., Homer, R. J., Ring, A., Wilen, C. B., and Iwasaki, A. (2020) Mouse model of SARS-CoV-2 reveals inflammatory role of type I interferon signaling. *J. Exp. Med.* **217**, e20201241
56. Meyer, L., Lopez, T., Espinosa, R., Arias, C. F., Vollmers, C., and DuBois, R. M. (2019) A simplified workflow for monoclonal antibody sequencing. *PLoS One* **14**, e0218717
57. Juste, M., Muzard, J., and Billiald, P. (2006) Cloning of the antibody kappa light chain V-gene from murine hybridomas by bypassing the aberrant MOPC21-derived transcript. *Anal. Biochem.* **349**, 159–161

SUPPORTING INFORMATION

for

Potent mouse monoclonal antibodies that block SARS-CoV-2 infection

Youjia Guo[1], Atsushi Kawaguchi[2,3,4], Masaru Takeshita[5], Takeshi Sekiya[2], Mikako Hirohama[2], Akio Yamashita[6], Haruhiko Siomi[1,*], Kensaku Murano[1,*]

[1]Department of Molecular Biology, Keio University School of Medicine, Tokyo, Japan
[2]Department of Infection Biology, Faculty of Medicine, University of Tsukuba, Tsukuba, Japan
[3]Transborder Medical Research Center, University of Tsukuba, Tsukuba, Japan
[4]Microbiology Research Center for Sustainability, University of Tsukuba, Tsukuba, Japan
[5]Division of Rheumatology, Department of Internal Medicine, Keio University School of Medicine, Tokyo, Japan
[6]Department of Molecular Biology, Yokohama City University School of Medicine, Yokohama, Japan

*Corresponding authors: kmurano@keio.jp (K.M.), awa403@keio.jp (H.S.)

Running Title: Mouse anti-SARS-CoV-2 spike monoclonal antibody
Keywords: SARS-CoV-2, spike, mouse monoclonal antibody, neutralizing antibody

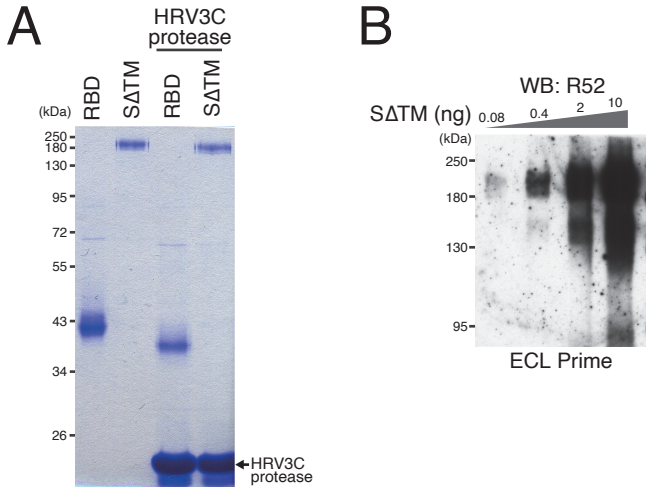
A
HRV3C protease
RBD
SΔTM
RBD
SΔTM
(kDa)
250
180
130
95
72
55
43
34
26
HRV3C protease
B
WB: R52
SΔTM (ng)
0.08
0.4
2
10
(kDa)
250
180
130
95
ECL Prime

Fig. S2

Guo *et al.*

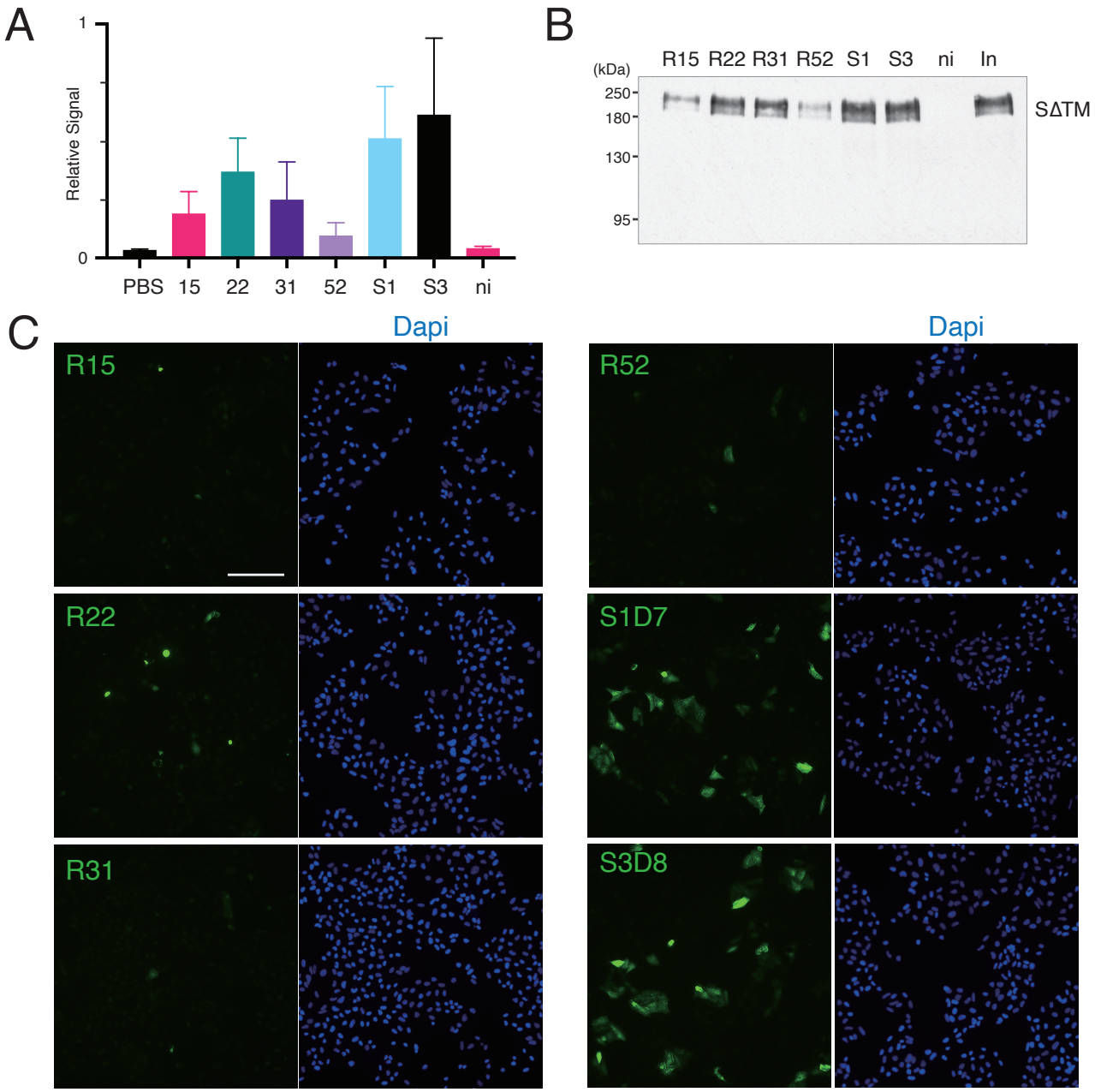

Fig. S3

Guo *et al.*

A

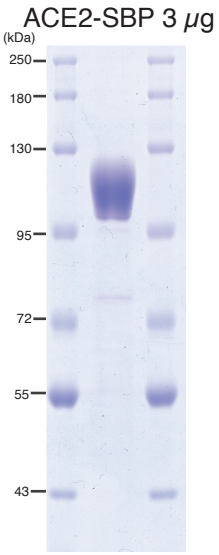

B

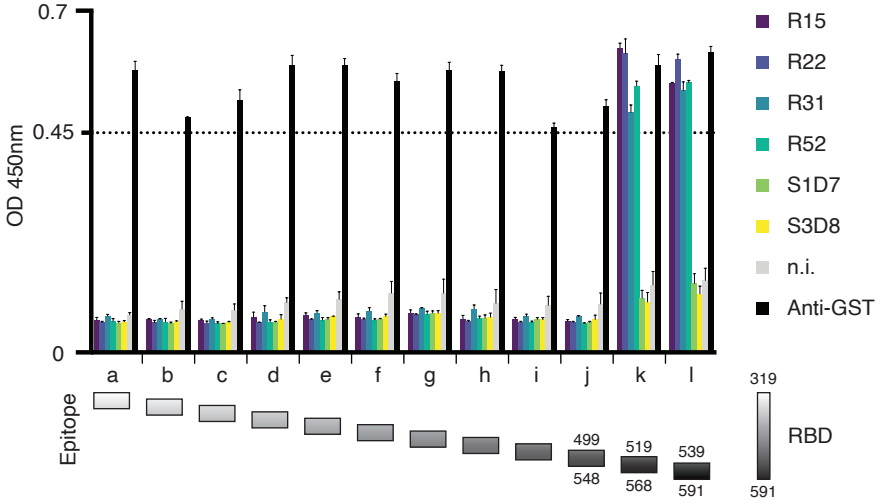

C

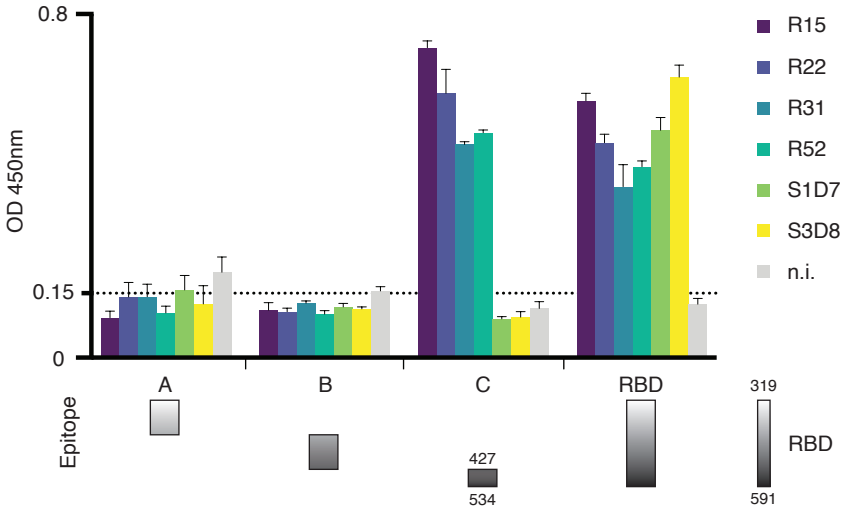

D

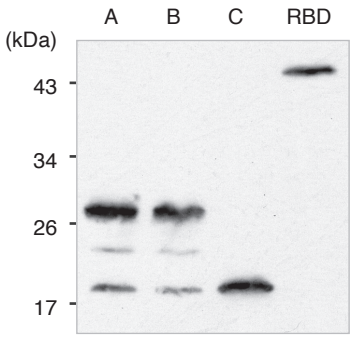

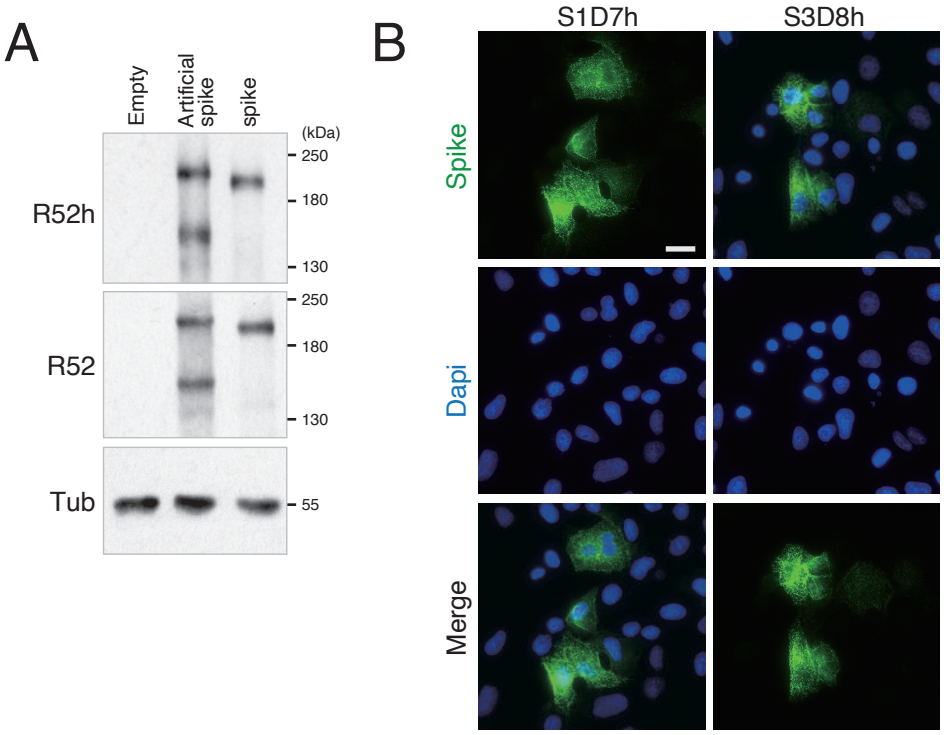
A
Empty
Artificial spike
spike
(kDa)
R52h
250
180
130
R52
250
180
130
Tub
55
B
S1D7h
S3D8h
Spike
Dapi
Merge

Table S1. Monoclonal antibodies neutralizing SARS-CoV-2 infection.

Clone	Host species	Cell line	Virus titer			IC_{50} (ng/ml)	Reference
			TCID50	PFU	FFU		
BD-368-2	Human	Vero	-	100	-	15	Cao *et al.*, Cell (17)
0304-3H3		VeroE6	100	-	-	110	Chi *et al.*, Science (19)
1B07*		VeroE6		-	100	37	Hassan *et al.*, Cell (28)
P2C-1F11		VeroE6	-	-	600	15	Ju *et al.*, Nature (22)
S309		VeroE6	-	-	100	79	Pinto *et al.*, Nature (26)
CC6.33		HeLa-ACE2	-	150	-	39	Roger *et al.*, Science (27)
CB6		VeroE6	-	-	-	36	Shi *et al.*, Nature (25)
47D11		VeroE6	100	-	-	570	Wang C *et al.*, Nat Commun (20)
B38		Vero	500	-	-	177 / 1,967	Wu *et al.*, Science (21)
COV2-2196		VeroE6	100 / 200	-	-	15	Zost *et al.*, Nature (29)
S1D7	Mouse	VeroE6/TM2	-	-	100	405.2	This paper
S3D8		VeroE6/TM2	1500	-	-	139	

*1B07 is a chimeric monoclonal antibody which combines mouse Fv and human Fc.

Table S2. Protein sequence of antibody variable regions.

Clone	Isotype	Chain	FR1	CDR1	FR2	CDR2	FR3	CDR3	FR4
R15	IgG1k	heavy	QIQLVQSGPELKKPGETVKISCKAS	GYTFTKYG	INWVKQAPGKDLKWMGW	INTYTGEP	AYGDDFKGRFAFSLETSTNTAYLQINNFKNEDTATYFC	ARNGAMDY	WGQGTSVTVSS
		kappa	DVVMTQNPLTLSVTIGQPASISCKSS	QSLLDSDGKTY	LIWLLQRPGQSPKRLIS	LVS	KLDSGVPDRFTGSGSGTDFTLKISRVEAEDLGVYYC	WQGTHFPGT	FGGGTKLEIK
R22	IgG2ak	heavy	EVQLQQSGPELVRPGASVKISCKTS	GYTFTEYI	IHWVKQSHGKSLEWIGG	IDPNNGDT	SYNQKFKGKASLTVDKSSSTAYMELRSLTSDDSAVYYC	ARLDFDY	WGQGTTLTVSS
		kappa	DIVMTQSHKFMSTSVGDRVSITCKAS	QDVRTA	VAWYQQKPGQSPKLLIY	WAS	TRYTGVPDRFTGSGSGTDYTLTISSVQAEDLALYYC	QQHDSTPLT	FGAGTKLELK
R31	IgG2bk	heavy	QVQLQQSGAELVRPGTSVKISCKAS	YTFTNYW	LAWVKQRPGHGLEWIGD	IYPGGAYT	NFNEKFKGKATLTADTSSSTAYMQLSSLTSEDSAVYFC	ARDGHYGYAMDY	WGQGTSVTVSS
		kappa	DIVMTQAAFSNPVTLGTSASISCRSS	KSLLHSNGITY	LYWYLQKPGQSPQLLIY	QMS	DLASGVPDRFSSSGSGTDFTLRISRVEAEDVGVYYC	AQNLELPRT	FGGGIKLEIK
R52	IgG1k	heavy	QIQLVQSGPELKKPGETVKISCKAS	GYTFTNYG	MNWVKQAPGNGLRWMGW	INTYTREP	SYAADFKGRFAFSLETSARAAYLQINNLKNEDTATYFC	ARNGAMDY	WGQGTSVTVSS
		kappa	DVVMTQTPLTLSVTFGQPASISCKSS	QSLLDSDGKTY	LIWLLQRPGQSPKRLIS	LVS	KLDSGVPDRFTGSGSGTDFTLKISRVEAEDLGVYYC	WQGTHFPGT	FGGGTKLEIK
S1D7	IgG2ak	heavy	QVQLQQSGAELVKPGASVKLSCKAS	GYTFTSYY	IYWMKQRPGQGLEWIGE	INPNNGGT	NFNEKFKSKATLTVDKSSSTAYMQLSSLTSEDSAVYYC	TRGHSDY	WGQGTTLTVSS
		kappa	DIVLTQSPASLAVSLGQRATISCRAS	ESVEYYGTGL	MQWYQQKPGQPPKLLIY	AAS	NVESGVPARFSGSGSGTDFSLNIHPVEEDDIAMYFC	QQTRKVPYT	FGGGTKLEIK
S3D8	IgG2ak	heavy	QVQLQQSGAELVKPGASVKLSCKAS	GYTFTSYY	MYWMKQRPGQGLEWIGE	INPSNGGT	NFNEKFKSKATLTVDKSSSTAYMQLSSLTSEDSAVYYC	TIFITRDAMDY	WGQGTSVTVSS
		kappa	QIVLTQSPAIMSASPGEKVTLTCSAS	SSVSSSY	LFWYQQKPGSSPKLWIY	TTS	NLASGVPARFSGSGSGTSYSLTISSMEAEDAASYFC	HQWSSYPPT	FGAGTKLELK

FR: frame region, CDR: complementarity determining region

Supplemental Figure Legends

Figure S1

A. Recombinant spike glycoproteins were treated with HRV3C protease to remove SBP-tag before immunizing mice.
B. Clone R52 showed the highest performance on western blotting among our antibodies and detected even 0.08 ng SΔTM glycoprotein.

Figure S2

A. Quantification of signal intensity of spike glycoprotein immunoprecipitated by monoclonal antibodies. S1, S1D7; S3, S3D8; ni, non-immune IgG. Error bars indicate standard deviation (n=3).
B. Monoclonal antibody clones S1D7 and S3D8 maintain high efficiency even in the presence of 0.1% SDS. S1, S1D7; S3, S3D8; ni, non-immune IgG; In, input.
C. Immunofluorescence (IF) staining of spike glycoprotein expressed in HeLa cells with all six monoclonal antibodies. S1D7 and S3D8 showed higher performance in IF. Images were captured using a Keyence BZ-X810 fluorescence microscope. Scale bar, 200 μm.
D. Expression of SARS-CoV-2 M protein in 293T cells. 293T cells were transfected with plasmid encoding SARS-CoV-2 M protein, followed by WB using anti-flag antibody.
E. Hela cells were transfected with plasmids encoding SARS-CoV-2 spike and M proteins, followed by IF using anti-spike (S1D7) and anti-flag antibodies. Scale bar, 20 μm.

Figure S3

A. ACE2-SBP protein was purified from the culture supernatant of Expi293F cells transfected with a plasmid encoding ACE2-SBP.

B. ELISA using monoclonal antibodies against small overlapping RBD segments. Clone R15, R22, R31, and R52 recognized spike protein RBD; a.a. 519-568 and a.a. 539-591, but not a.a. 499-548, indicating a continuous epitope within overlapping a.a. 549-568. Clone S1D7 and S3D8 failed to recognize all small overlapping RBD segments. Error bars indicate standard deviation (n=3).

C. ELISA using monoclonal antibodies against 6×His-tagged RBD segments secreted in the culture medium of 293T cells. Clone R15, R22, R31, and R52 recognized spike protein RBD segment C, which contains continuous epitope a.a. 549-568. Clone S1D7 and S3D8 failed to recognize all RBD segments, suggesting that they require an intact RBD tertiary structure to bind spike protein. Error bars indicate standard deviation (n=3).

D. 6×His-tagged RBD segments were secreted in the culture medium of 293T cells and detected by western blotting.

Figure S4

A. R52h is applicable for WB. Lysates of 293T cells expressing artificial spikes carrying T4 foldon or wild-type spike glycoproteins were separated by SDS-PAGE, followed by WB using human/mouse chimeric antibody R52h which was secreted by 293T cells.

B. S1D7h and S3D8h are applicable for IF. Spike glycoprotein expressed in HeLa cells was stained with human/mouse chimeric antibody S1D7h or S3D8h which were secreted by 293T cells. Scale bar, 20 μm.

Detailed Experimental Procedures

Expression and purification of proteins in human cells

Synthetic DNA sequences encoding SARS-CoV-2 spike protein ectodomain (SΔTM, residue 1-1208; strain Wuhan-hu-1; GenBank: QHD43416.1) and RBD (residue 319-591; strain Wuhan-hu-1; GenBank: QHD43416.1) fused with an N-terminal signal peptide, a C-terminal trimerization motif, an HRV3C cleavage site, an SBP purification tag, and an 8xHis-tag were inserted into pEFx mammalian expression vector. S1/S2 (682-RRAR-685) and S2' (986-KV-987) cleavage sites of spike protein were mutated (682-GSAS-685, 986-PP-987, respectively) to prevent protease cleavage. The codon composition of DNA fragments was optimized and synthesized for protein expression in human cells (FASMAC). Full-length spike, human ACE2-SBP (residue 1-708; NP_001358344), and ACE2-FLAG were synthesized and cloned into pcDNA3.4 vector (Thermo Fisher). Recombinant proteins were prepared by Expi293 Expression System (Thermo Fisher) according to the manufacturer's instruction. They were secreted into culture medium supernatant of the Expi293F cells, and then affinity purified by Streptavidin Sepharose High Performance (Cytiva). Purification tags were removed by treating recombinant proteins with HRV3C protease (TaKaRa) and cOmplete™ His-tag Purification Resin (Roche). Purity and glycosylation of recombinant proteins were examined by PNGase F (N-Zyme Scientifics) treatment followed by SDS-PAGE and Coomassie staining. The containment measures for the living modified organisms in all experiments were confirmed by the Ministry of Education, Culture, Sports, Science and Technology of Japan on April 27, 2020.

Expression and purification of proteins in *E. coli*

The DNA sequence encoding SARS-CoV-2 spike protein RBD (residue 410-580; strain Wuhan-hu-1; GenBank: QHD43416.1) was amplified from a nasopharyngeal swab of a patient treated in the Keio University Hospital, and in-framed inserted into pGEX-5X-1 and pMAL-c2G *E. coli* expression plasmid, downstream of GST-tag and MBP-tag encoding sequence respectively. Sample collection from a patient is approved by Keio University Bioethics Committee with the number 20200063 and abide by the Declaration of Helsinki Principles. Recombinant proteins were expressed in overnight 16ºC cultured BL21(DE3)pLysS competent cells transformed by corresponding vector under induction of 1 mM Isopropyl β-D-1-thiogalactopyranoside (IPTG). MBP-tagged RBD was affinity purified by Amylose Resin (NEB) according to manufacturer's instructions; GST-tagged RBD was affinity purified by Glutatione Sepharose 4B (Cytiva) according to manufacturer's instructions. Purity of purified recombinant proteins were examined by SDS-PAGE followed by Coomassie staining.

Cell cultures

The mouse myeloma cell line SP2/0-Ag14 (RCB0209) was provided by the Riken Bioresouces Center (Tsukuba, Japan). The cells were cultured in RPMI 1640 (Nissui) supplemented with 10% heat-inactivated calf serum (Biowest) and 1 ng/mL recombinant human interleukin 6 (IL-6, PeproTech). HeLa and 293T cells were cultured in DMEM (Nacalai tesque) with 10% fetal bovine serum (Biowest). We maintained hybridoma clones against spike glycoproteins in Hybridoma Serum-free Medium (FUJIFILM Wako) supplemented with 1 ng/mL IL-6.

Production of monoclonal antibodies

BALB/c mice were immunized twice in 3-week intervals, with the second immunization serving as a booster. Mice were injected intraperitoneally with 100 μL chyle containing 10-50 μg antigen prepared with TiterMax Gold adjuvant (Sigma-Aldrich) according to the manufacturer's instructions. Four days after boosting, splenocytes of immunized mice were collected by grinding the spleens in RPMI 1640 medium. Splenocytes (1×10^8) were immediately mixed with 5×10^7 SP2/0 myeloma cells and fused using an electro cell fusion generator ECFG21 (NepaGene) according to the manufacturer's instructions. After fusion, cells were cultured in HAT medium (RPMI 1640 supplemented with 10% calf serum containing HT supplement (Gibco) and 0.4 μM aminopterin (Sigma-Aldrich)) for 10 days to select hybridomas. Hybridomas were subsequently screened by ELISA, in which RBD glycoproteins were generated from the Expi293F expression system. We performed western blotting and immunoprecipitation for further screening and subjected to monoclonization by serial dilution. For antibody production, monoclonal hybridomas were cultured in Hybridoma Serum-Free Medium (FUJIFILM Wako) supplemented with IL-6. Monoclonal antibodies were purified from hybridoma culture supernatants using Thiophilic-Superflow Resin (Clontech) or Ab-Capcher MAG2 (ProteNova) according to the manufacturer's instructions. The isotype of antibodies was determined using the IsoStrip Mouse Monoclonal Antibody Isotyping Kit (Roche).

Western blotting and immunoprecipitation

SΔTM and RBD glycoproteins were resolved on SDS-PAGE and transferred onto a nitrocellulose membrane (Amersham Protran, GE Healthcare). Lysates of 293T

cells transfected with plasmids encoding full-length spike glycoproteins was also separated by SDS-PAGE for WB. The membrane was blocked in 1% nonfat skim milk and then incubated in 1 μg/mL anti-spike antibodies for 1h at room temperature. After three times washing in PBS-T (0. 1% Tween 20), the membrane was incubated in 1:5000 dilution of the peroxidase-conjugated sheep anti-mouse IgG secondary antibody (MP Biomedicals) for 30 min at room temperature. Signals were detected using ECL Western Blotting Detection Reagents (GE Healthcare).

For immunoprecipitation assay, 1 μg of purified antibodies was conjugated to 10 μl Dynabeads Protein G (Thermo Fisher) for 30 min at room temperature, followed by washing twice in IP buffer (20 mM Tris-HCl(pH 7.4), 150 mM NaCl, 0.1% NP-40). Antibody conjugated beads were incubated with 100 ng SΔTM in 50 μl IP buffer for 2 hours at room temperature. Beads were washed three times in IP buffer and eluted with SDS-PAGE loading dye at 95ºC for 5 min. Immunoprecipitation of SΔTM was examined by SDS-PAGE followed by western blotting using antibody R52.

Immunofluorescence

Before performing immunofluorescence, HeLa cells seeded on cover glasses were transfected with plasmids encoding full length SARS-CoV-2 spike protein for 2 days using Lipofectamine 2000 (Thermo Fisher). Cells were fixed with 2% formaldehyde in PBS for 10 min at room temperature, washed in PBS-T once, and permeabilized with 0.1% Triton X-100 in PBS for 10 min at room temperature. Cells were blocked by 1% non-fat skim milk in PBS-T for 10 min, then incubated with 0.5 μg/mL antibody for 1 h at room temperature. After three times wash in PBS-T, cells were incubated in 1:500 diluted Alexa Fluor 488 conjugated goat anti-mouse IgG secondary antibody (Thermo

Fisher) and 1 μg/mL DAPI solution for 30 min at room temperature. The cover glasses were mounted with Prolong Glass Antifade Mountant (Thermo Fisher) overnight at room temperature before observing. The fluorescence images were taken with Keyence BZ-X810 fluorescence microscope and Olympus FV3000 confocal laser scanning microscope.

ELISA of antibody binding to SARS-CoV-2 spike protein

Nunc MaxiSorp™ flat-bottom 96-well plates (Thermo Fisher) were coated with 170 ng SΔTM in 50 μl PBS overnight at 4ºC, then blocked at room temperature for 1 hour by applying 200 μl of 3.75% BSA in PBS-T. Monoclonal antibodies starting from 100 μg/mL were four-folds serial diluted with blocking buffer to 12 gradients and incubated with plates for 1 hour at room temperature, followed by incubation with horseradish peroxidase (HRP) conjugated sheep anti-mouse secondary antibody (MP Biomedicals) 1:5000 diluted in blocking buffer for 30 min at room temperature. Plates were incubated for 15 min at room temperature with 1-Step Turbo TMB-ELISA Substrate Solution (Thermo Fisher), then terminated with equal volume of 1M phosphoric acid. Signal was quantified by measuring absorbance at 450 nanometer using iMark Microplate Absorbance Reader (Bio-Rad Laboratories). Half-maximum effective concentration (EC_{50}) was calculated by non-linear regression analysis of absorbance curve.

Epitope mapping of monoclonal antibody

For small overlapping RBD segments, the respective DNA sequences encoding spike protein residues 319-368, 339-388, 359-408, 379-428, 399-448, 419-468, 439-488, 459-508, 479-528, 499-548, 519-568, and 539-591 were subcloned from full-length spike

protein coding sequence, and in-framed inserted into pGEX-5X-1 *E. coli* expression plasmid, downstream of GST-tag encoding sequence. Recombinant proteins were expressed in 3 mL of 37 ºC overnight cultured BL21(DE3)pLysS cells transformed by the corresponding plasmid under induction of MagicMedia *E. coli* Expression Medium (Thermo Fisher). Cells were washed once and lysed in 250 μL PBS by sonication, 5 times diluted with PBS, then applied 50 μL per well in a 96 well plate as antigen in ELISA for epitope mapping.

For RBD segments secreted by 293T cells, the respective DNA sequences encoding spike protein residue 319-426, 427-534, and 535-591 were subcloned from full-length spike protein coding sequence, and in-framed inserted into pEFx mammalian expression plasmid, downstream of sequence encoding an N-terminal signal peptide followed by a 6×His-tag, an SBP-tag, and an HRV3C cleavage site. Recombinant proteins were expressed by transfecting 293T cells at a starting number of 1×10^6 cells in a 6 cm culture dish with the corresponding plasmid using Lipofectamine 2000 (Thermo Fisher). Three days after transfection, culture supernatants were collected and filtered by 0.45 μm filter, and then 50 μL of each antigen was applied for epitope mapping per well in ELISA.

ACE2-binding inhibition assay

For spike pull-down assay, SΔTM glycoprotein was incubated with 1 μg anti-spike antibody in 50 μl binding buffer (PBS supplemented with 0.1% NP-40) at room temperature for 1 hour, then 3 μg of ACE2-SBP recombinant protein was applied the reaction for 1 hour. The ACE2-SBP was pull-down by 10 μl Dynabeads M-270 Streptavidin (Thermo Fisher) for 30 min at room temperature, followed by washing twice with binding buffer and elution with SDS-PAGE loading dye at 95ºC for 5 min. ACE2-

Spike binding inhibition was examined by SDS-PAGE, followed by WB using antibody R52.

For bead-based neutralization assay, 20 µl of Streptavidin beads were incubated with 4 µg of RBD-SBP in 100 µl of TBSTx (TBS supplemented with 1% TritonX-100) overnight at 4°C with shaking. After washing, beads were incubated with diluted antibodies for 20 min at 4°C, washed, incubated with 4 µg/mL of ACE2-FLAG for 20 min at 4°C, washed, and incubated with an anti-DYKDDDDK antibody conjugated with APC fluorophore (MBL) for 20 min at 4°C. After the final wash, the mean fluorescence intensity (MFI) of beads was analyzed by a FACS Verse (BD). The relative MFI of beads was calculated by normalization using the MFI of beads incubated with non-immune mouse IgG.

Virus neutralization assay

SARS-CoV-2 virus (obtained from the National Institute of Infectious Diseases) was prepared from culture fluids harvested from infected VeroE6/TMPRSS2 cells (JCRB Cell Bank, JCRB1819) (41). The virus titer was 3×10^7 $TCID_{50}$/mL. The virus solution containing 1500 $TCID_{50}$ was incubated with each antibody at concentrations of serial threefold dilutions starting from 5 µg/mL. After incubating at room temperature for 1 h, the antibody-treated virus solution was mixed with VeroE6/TMPRSS2 cells in glass-bottom 96-well plates. At 7 h post-infection, cells were fixed in 4% PFA and subjected to indirect immunofluorescence assays using S1D7 antibody as described above. The number of infected cells were imaged and analyzed using ArrayScan (Thermo Fisher). Mouse anti-FLAG M2 antibody (Sigma) was also used as a control. Experiments with SARS-CoV-2 were performed in a biosafety level 3 (BSL3) containment laboratory at

University of Tsukuba.

Sequencing of antibody variable regions

Sequencing of antibody variable regions was carried out as described previously (56). Total RNA was extracted from the hybridoma cells using ISOGEN (NIPPON GENE) according to the manufacturer's instructions. 5' RACE (rapid amplification of 5' cDNA ends) was performed by the SMARTscribe Reverse Transcriptase kit (Clontech) in the presence of a Template-switch oligonucleotide (5'-AAGCAGTGGTATCAACGCAGAGTACATrGrGrG-3') containing three riboguanines (rGrGrG) at its 3' end. First-strand cDNA for heavy chain and kappa chain were synthesized using reverse RT primers, mIGHG_RT (5'-AGCTGGGAAGGTGTGCACAC-3') and mIGK_RT (5'-TTGTCGTTCACTGCCATCAATC-3'), respectively. cDNA for the heavy chain was amplified by PCR using universal forward primer, ISPCR (5'-AAGCAGTGGTATCAACGCAGAG-3'), and mIGHG_PCR primer (5'-GGGATCCAGAGTTCCAGGTC-3'), followed by Sanger sequencing. For the kappa chain, cDNA was amplified by PCR using ISPCR and mIGK_PCR primers (5'-ACATTGATGTCTTTGGGGTAGAAG-3'), and cloned into an *Eco*R V site of the pCAGGS-3Flag vector, followed by Sanger sequencing. The cloning step is required to sequencing the kappa light chain since a hybridoma cell line derived from myeloma SP2/0-Ag14 expresses an endogenous and aberrant kappa mRNA (GenBank Accession No. M35669) (57).

Expression of chimeric human/mouse anti-spike antibodies

The kappa and heavy chain variable regions were amplified and individually cloned by NEBuilder (NEB) into pcDNA3.4 carrying the constant regions of human IgG1. Recombinant antibodies were prepared by Expi293 Expression System (Thermo Fisher) according to the manufacturer's instruction. They were secreted into culture medium supernatant of the Expi293F cells, and then affinity purified by Ab-Capcher MAG2 (ProteNova). Recombinant antibodies were also secreted from commonly used 293T cells, into which the plasmids for heavy and light chains were co-transfected at a ratio of 1:2 by polyethylenimine. The culture supernatants containing antibodies were available for WB (R52h) and IF (S1D7h), detecting spike glycoprotein expressed in 293T or HeLa cells. The peroxidase-conjugated goat anti-human IgG (H+L) (Jackson ImmunoResearch) and Alexa Fluor 488 conjugated goat anti-human IgG (H+L) (Thermo Fisher) were used as secondary antibodies for WB and IF, respectively.